

Flow effects in the laser-induced thermal loading of optical traps and optofluidic devices

B. del Rosal,¹ C. Sun,² Y. Yan,³ M.D. Mackenzie,⁴ C. Lu,⁵ A. A. Bettiol,^{3,6} A.K. Kar,^{4,*} and D. Jaque¹

¹*Fluorescence Imaging Group, Departamento de Física de Materiales, Facultad de Ciencias, Universidad Autónoma de Madrid, Campus de Cantoblanco. Madrid 28049, Spain*

²*School of Biomedical Engineering and Sciences, Virginia Tech-Wake Forest University, Blacksburg, Virginia 24061, USA*

³*Singapore Institute for Neurotechnology, National University of Singapore 117456, Singapore*

⁴*Non-Linear Optics Group, Institute of Photonics and Quantum Sciences, School of Engineering and Physical Sciences, Heriot Watt University, Edinburgh EH14 4AS, UK*

⁵*Department of Chemical Engineering, Virginia Tech, Blacksburg, Virginia 24061, USA*

⁶*Department of Physics, National University of Singapore, 2 Science Dr 3, Singapore 117542, Singapore*

a.k.kar@hw.ac.uk

Abstract: Flow effects on the thermal loading in different optofluidic systems (optical trap and various microfluidic channels) have been systematically explored by using dye-based ratiometric luminescence thermometry. Thermal images obtained by fluorescence microscopy demonstrate that the flow rate plays a key role in determining both the magnitude of the laser-induced temperature increment and its spatial distribution. Numerical simulations were performed in the case of the optical trap. A good agreement between the experimental results and those predicted by mathematical modelling was observed. It has also been found that the dynamics of thermal loading is strongly influenced by the presence of fluid flow.

©2014 Optical Society of America

OCIS codes: (280.6780) Temperature; (300.6280) Spectroscopy, fluorescence and luminescence.

References and links

1. C. Monat, P. Domachuk, and B. Eggleton, "Integrated optofluidics: A new river of light," *Nat. Photonics* **1**(2), 106–114 (2007).
2. D. Psaltis, S. R. Quake, and C. Yang, "Developing optofluidic technology through the fusion of microfluidics and optics," *Nature* **442**(7101), 381–386 (2006).
3. X. Fan and I. M. White, "Optofluidic microsystems for chemical and biological analysis," *Nat. Photonics* **5**(10), 591–597 (2011).
4. B. S. Schmidt, A. H. Yang, D. Erickson, and M. Lipson, "Optofluidic trapping and transport on solid core waveguides within a microfluidic device," *Opt. Express* **15**(22), 14322–14334 (2007).
5. A. H. Yang, S. D. Moore, B. S. Schmidt, M. Klug, M. Lipson, and D. Erickson, "Optical manipulation of nanoparticles and biomolecules in sub-wavelength slot waveguides," *Nature* **457**(7225), 71–75 (2009).
6. D. Di Carlo, D. Irimia, R. G. Tompkins, and M. Toner, "Continuous inertial focusing, ordering, and separation of particles in microchannels," *Proc. Natl. Acad. Sci. U.S.A.* **104**(48), 18892–18897 (2007).
7. A. Y. Lau, L. P. Lee, and J. W. Chan, "An integrated optofluidic platform for Raman-activated cell sorting," *Lab Chip* **8**(7), 1116–1120 (2008).
8. X. Cui, L. M. Lee, X. Heng, W. Zhong, P. W. Sternberg, D. Psaltis, and C. Yang, "Lensless high-resolution on-chip optofluidic microscopes for *Caenorhabditis elegans* and cell imaging," *Proc. Natl. Acad. Sci. U.S.A.* **105**(31), 10670–10675 (2008).
9. M. Dienerowitz, M. Mazilu, and K. Dholakia, "Optical manipulation of nanoparticles: a review," *J. Nanophotonics* **2**, 021875 (2008).
10. H. Xin, X. Li, and B. Li, "Massive photothermal trapping and migration of particles by a tapered optical fiber," *Opt. Express* **19**(18), 17065–17074 (2011).
11. M. P. MacDonald, G. C. Spalding, and K. Dholakia, "Microfluidic sorting in an optical lattice," *Nature* **426**(6965), 421–424 (2003).
12. T. R. Kießling, R. Stange, J. A. Käs, and A. W. Fritsch, "Thermorheology of living cells—impact of temperature variations on cell mechanics," *New J. Phys.* **15**(4), 045026 (2013).

13. P. Haro-González, W. T. Ramsay, L. M. Maestro, B. del Rosal, K. Santacruz-Gomez, M. del Carmen Iglesias-de la Cruz, F. Sanz-Rodríguez, J. Y. Chooi, P. R. Sevilla, M. Bettinelli, D. Choudhury, A. K. Kar, J. G. Solé, D. Jaque, and L. Paterson, "Quantum Dot-Based Thermal Spectroscopy and Imaging of Optically Trapped Microspheres and Single Cells," *Small* **9**(12), 2162–2170 (2013).
14. V. Miralles, A. Huerre, F. Malloggi, and M.-C. Jullien, "A Review of Heating and Temperature Control in Microfluidic Systems: Techniques and Applications," *Diagnostics* **3**(1), 33–67 (2013).
15. S. Ebert, K. Travis, B. Lincoln, and J. Guck, "Fluorescence ratio thermometry in a microfluidic dual-beam laser trap," *Opt. Express* **15**(23), 15493–15499 (2007).
16. M. S. Jaeger, T. Mueller, and T. Schnelle, "Thermometry in dielectrophoresis chips for contact-free cell handling," *J. Phys. D Appl. Phys.* **40**(1), 95–105 (2007).
17. R. K. P. Benninger, Y. Koç, O. Hofmann, J. Requejo-Isidro, M. A. A. Neil, P. M. W. French, and A. J. DeMello, "Quantitative 3D mapping of fluidic temperatures within microchannel networks using fluorescence lifetime imaging," *Anal. Chem.* **78**(7), 2272–2278 (2006).
18. C. D. S. Brites, P. P. Lima, N. J. O. Silva, A. Millán, V. S. Amaral, F. Palacio, and L. D. Carlos, "Thermometry at the nanoscale," *Nanoscale* **4**(16), 4799–4829 (2012).
19. D. Jaque and F. Vetrone, "Luminescence nanothermometry," *Nanoscale* **4**(15), 4301–4326 (2012).
20. D. Ross, M. Gaitan, and L. E. Locascio, "Temperature measurement in microfluidic systems using a temperature-dependent fluorescent dye," *Anal. Chem.* **73**(17), 4117–4123 (2001).
21. R. Samy, T. Glowdel, and C. L. Ren, "Method for microfluidic whole-chip temperature measurement using thin-film poly(dimethylsiloxane)/Rhodamine B," *Anal. Chem.* **80**(2), 369–375 (2008).
22. C. D. S. Brites, P. P. Lima, N. J. O. Silva, A. Millán, V. S. Amaral, F. Palacio, and L. D. Carlos, "A Luminescent Molecular Thermometer for Long-Term Absolute Temperature Measurements at the Nanoscale," *Adv. Mater.* **22**(40), 4499–4504 (2010).
23. C. D. Brites, P. P. Lima, N. J. Silva, A. Millán, V. S. Amaral, F. Palacio, and L. D. Carlos, "Ratiometric highly sensitive luminescent nanothermometers working in the room temperature range. Applications to heat propagation in nanofluids," *Nanoscale* **5**(16), 7572–7580 (2013).
24. D. Choudhury, D. Jaque, A. Rodenas, W. T. Ramsay, L. Paterson, and A. K. Kar, "Quantum dot enabled thermal imaging of optofluidic devices," *Lab Chip* **12**(13), 2414–2420 (2012).
25. B. del Rosal, C. Sun, D. N. Loufakis, C. Lu, and D. Jaque, "Thermal loading in flow-through electroporation microfluidic devices," *Lab Chip* **13**(15), 3119–3127 (2013).
26. J. Sakakibara and R. J. Adrian, "Whole field measurement of temperature in water using two-color laser induced fluorescence," *Exp. Fluids* **26**(1-2), 7–15 (1999).
27. R. Osellame, H. J. W. M. Hoekstra, G. Cerullo, and M. Pollnau, "Femtosecond laser microstructuring: an enabling tool for optofluidic lab-on-chips," *Laser Photon. Rev.* **5**(3), 442–463 (2011).
28. K. Sugioka and Y. Cheng, "Integrated microchips for biological analysis fabricated by femtosecond laser direct writing," *MRS Bull.* **36**(12), 1020–1027 (2011).
29. H. Mao, J. Ricardo Arias-Gonzalez, S. B. Smith, I. Tinoco, Jr., and C. Bustamante, "Temperature Control Methods in a Laser Tweezers System," *Biophys. J.* **89**(2), 1308–1316 (2005).
30. G. Baffou, R. Quidant, and F. J. García de Abajo, "Nanoscale Control of Optical Heating in Complex Plasmonic Systems," *ACS Nano* **4**(2), 709–716 (2010).
31. D. K. Cai, A. Neyer, R. Kuckuk, and H. M. Heise, "Optical absorption in transparent PDMS materials applied for multimode waveguides fabrication," *Opt. Mater.* **30**(7), 1157–1161 (2008).

1. Introduction

The combination of microfluidic and optical elements in a single platform, and the subsequent development of so-called optofluidic devices has become an emergent research field in the last few years [1–3]. Optofluidic devices are compact platforms that allow for the optical manipulation and study of microsized elements in a fully controlled environment (fluid). Optofluidic devices have already been demonstrated to be effective tools for the study and manipulation of inert (microspheres, nanoparticles) and living (cells and small organisms) objects [4–8]. In most cases, manipulation is achieved by taking advantage of the optical forces that appear in the vicinity of tightly or weakly focused laser beams. These forces could be related either to the presence of thermal gradients or to photon-particle momentum exchange and light induced particle polarizability [9–11]. In general, laser radiation is partially absorbed by the liquid in which the manipulated particles are suspended and, as a consequence of this absorption, the creation of the optical gradient is accompanied by the creation of a thermal gradient. The spatial extension and magnitude of the laser-induced temperature distribution in the optofluidic device is of great importance. First, the existence of such thermal gradients would lead to the creation of convection currents and this, in turn, could prevent particles from being appropriately trapped and manipulated. Temperature is

even more critical when dealing with biological samples, such as single cells, as their biochemical properties would be strongly affected by any laser-induced heating [12]. For instance, a temperature increment beyond the cytotoxic level (>42 °C) can result in irreversible cell damage. In most of the experiments dealing with optical trapping of microparticles, only tens of milliwatts are required for efficient trapping. Nevertheless, when dealing with optical trapping of living cells, the required powers are larger. For instance, the creation of an optical force close to 20 pN in a living lymphocyte requires a pump power close to 100 mW and for such a laser power, laser-induced heating could be as large as 5 °C [13]. This means that, if experiments are carried out at 37 °C, trapping laser could heat the living cell up to 42 °C and, as mentioned, induce irreversible damage during trapping. Temperature control is critical for a great number of applications of optofluidic devices [14], which would benefit from an exact knowledge of the internal temperature distribution. Some previous works have already reported on the acquisition of thermal images of microfluidic devices but, in most cases, they were obtained only in static conditions (that is, under no applied fluid flow), and in the cases where a flow was applied, its effect on the temperature distribution was not analyzed [15–17]. Nevertheless, most optofluidic systems require the establishment of a controlled fluid flow for particle control and manipulation. In the presence of a heating source, such as partially absorbed laser beams, fluid flow is expected to induce heat dissipation so that the magnitude and stabilization time of thermal loading in the presence of fluid flow could be significantly different to that produced under static conditions. Furthermore, the presence of fluid flow could also affect the shape of the temperature distributions inside optofluidic devices, making them become highly asymmetric. Despite its relevance, the role played by fluid flow in the thermal distributions created in optofluidic devices has not yet been studied.

Measuring temperature in microfluidic devices under real operating conditions is quite a challenging task. Conventional techniques are not useful in such systems, as their reduced dimensions make it impossible to accurately determine the temperature inside the microchannels without producing a significant disturbance in the properties of the setup. One of the easiest ways to overcome this problem is luminescence thermometry, demonstrated to be useful in the study of a great number of fluorescent systems [18]. This technique is based on the incorporation in the microfluidic device of luminescent probes, whose emission properties are strongly temperature-dependent [19]. Remote thermal sensing can be achieved through analysis of the intra-channel luminescence signal, as has already been demonstrated in a number of works in the literature [16, 20–24]. Different luminescent probes, such as quantum dots, polymers and dyes have been used. The approach used in this work, where a solution of two fluorescent dyes is used as a thermal probe, has proven to be particularly effective for the thermal characterization of microfluidic systems [15, 25]. The luminescence of Rhodamine B, which suffers a strong thermal quenching, allows for thermal sensing from a simple intensity analysis. However, any local fluctuations in dye concentration or in the optical excitation intensity would result in emission intensity changes not related to temperature, thus reducing the accuracy of the approach. Fortunately, it is possible to overcome this obstacle in different ways, for instance, by using fluorescence lifetime measurements [17], instead of fluorescence intensity or by incorporating a reference dye with a temperature-independent luminescence (as is the case of Rhodamine 110) to the temperature-sensitive dye solution. This makes it possible to calculate the temperature as a function of the ratio of the emissions of both dyes, thus avoiding any possible undesired effects due to local variations in the dye densities (such as fluid compression) as these effects would affect equally both dyes [26]. In addition, a continuous flow of the dye solution can be easily established through a microfluidic channel, thus making it a suitable thermal probe to study the dynamics of thermal loading in microfluidics as the temperature measurement is not limited to static situations. Moreover, high-resolution temperature distribution maps in microfluidic systems can be obtained with this method when a fluorescence microscope

capable of a spatial analysis of the luminescence is used. In this work, a thermosensitive dye solution has been used in order to perform a systematic investigation of both the magnitude and spatial distribution of laser-induced thermal loading in a variety of optofluidic systems, exploring the effect of the applied flow. As an optical trap constitutes the simplest case of interaction between a light source and a fluid, the effects of flow on the thermal loading in this system have been extensively studied and compared to those predicted by mathematical modelling. Once the validity of the experimental procedure has been demonstrated through the good agreement between simulations and experimental results, other optofluidic devices including those designed for optical sorting, trapping and stretching have been studied in the same way.

2. Experimental

2.1 Device fabrication

Laser-induced thermal loading was studied in four different optofluidic systems that are schematically represented in Fig. 1. The microchannel used for the vertical optical trapping experiments (100 μm in depth), shown in Fig. 1(a), was provided by Ibidi, Inc. (μ -Slide 0.1 Luer). In this case, optical trapping was achieved in a “standard” geometry by focusing a 980 nm laser beam in the middle of the channel, as is schematically depicted in the figure. We have also investigated the laser-induced temperature distributions in optofluidic devices designed for optical trapping in a lateral configuration (Fig. 1(b)). Laser radiation (980 or 1480 nm) delivered by a multimode fiber was focused into the channel by using a built-in lens (see curved sections fabricated in the PDMS on Figs. 1(b) and 1(c)). Figure 1(c) shows the schematic representation of an optofluidic device designed for laser sorting of microparticles. It consists of two identical and parallel channels with a common section interconnecting them. A laser beam focused in the middle of this area is used to modify the trajectories of the microparticles by using radiation related scattering forces. The particle sorting was experimentally achieved by using a single-mode fiber coupled 980 nm laser focused by a built-in microlens. The devices schematically represented in Figs. 1(b) and 1(c) were both fabricated on PDMS using a standard soft lithography method. Briefly, photomasks were fabricated on 3 in. silicon wafers based on microscale patterns designed with computer-aided design software (AutoCAD). A 5-mm-thick layer of prepolymer mixture was poured onto the master and then cured in an oven for at least 6 hours at 65 $^{\circ}\text{C}$. The baked PDMS replicas were then peeled from the master, punched for inlet and outlet holes, oxidized by plasma treatment and bonded to a pre-cleaned and oxidized glass slide. The size of the microchannels was the same in both chips and set to 50 μm in width and 70 μm in depth.

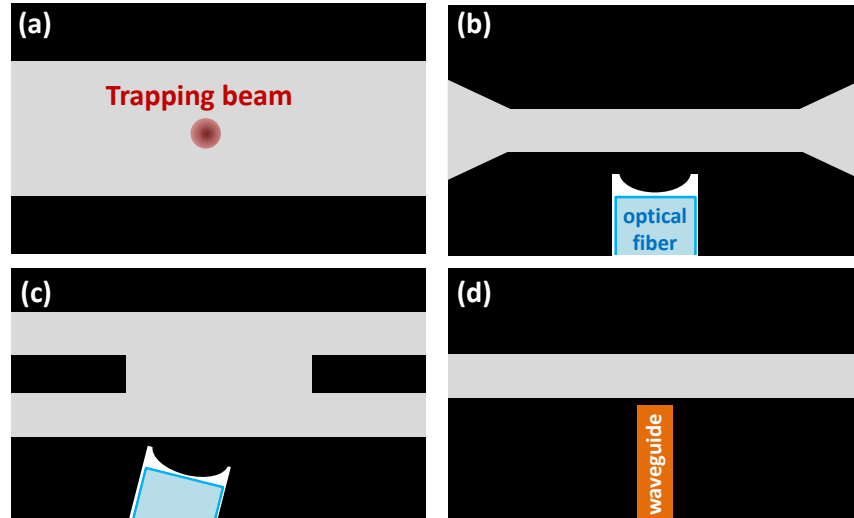


Fig. 1. Schematic representation of the four devices used in this work: (a) 100 μm deep microchannel for particle trapping; (b) 50x70 μm channel illuminated from one side by a multimode optical fiber; (c) 70 μm deep microchannel for particle sorting; (d) monolithic device with an integrated waveguide.

Finally, we have also investigated the thermal loading in monolithic optofluidic devices (see Fig. 1(d)). They were fabricated on fused silica by ultrafast laser inscription followed by selective chemical etching, which has proven to be a useful microfabrication technique in optofluidics [27, 28]. The fabrication procedure of the chips used here is described in detail in previous works [24]. Briefly, the optical waveguide and microchannels were simultaneously fabricated by applying 460 fs laser pulses at 1047 nm with a repetition rate set at 500 kHz. After inscription, the devices were etched for 12 hours in a hydrofluoric acid solution (10% dilution in deionised water). The waveguide was polished to reveal the facet, which was then bonded to a single-channel fiber array (Opteron Co.) using conventional UV curing (i.e. an UV curable epoxy). Two chips with different widths (25 μm and 35 μm) and heights (37 μm and 47 μm) were fabricated.

2.2 Temperature measurement

In order to achieve thermal sensing and time-resolved imaging in the different optofluidic devices, we used an aqueous solution of two fluorescent dyes: Rhodamine B (RhB), whose emission is strongly quenched with increasing temperature; and Rhodamine 110 (Rh110), which acts as a reference dye (it shows a negligible thermal fluorescence quenching). Both dyes were provided by SigmaTech Inc. and the concentrations in the solution were set to 0.25 mM and 0.05 mM for RhB and Rh110, respectively. At this point, it should be noted that these concentrations were selected to ensure a similar emitted intensity for both dyes so that thermal measurements were easier. A continuous flow of the fluorescent dye solution was established through the different devices by connecting them to a syringe pump (NE-1002X Programmable Microfluidics Syringe Pump from New Era Pump Systems Inc.) via PFA plastic tubing.

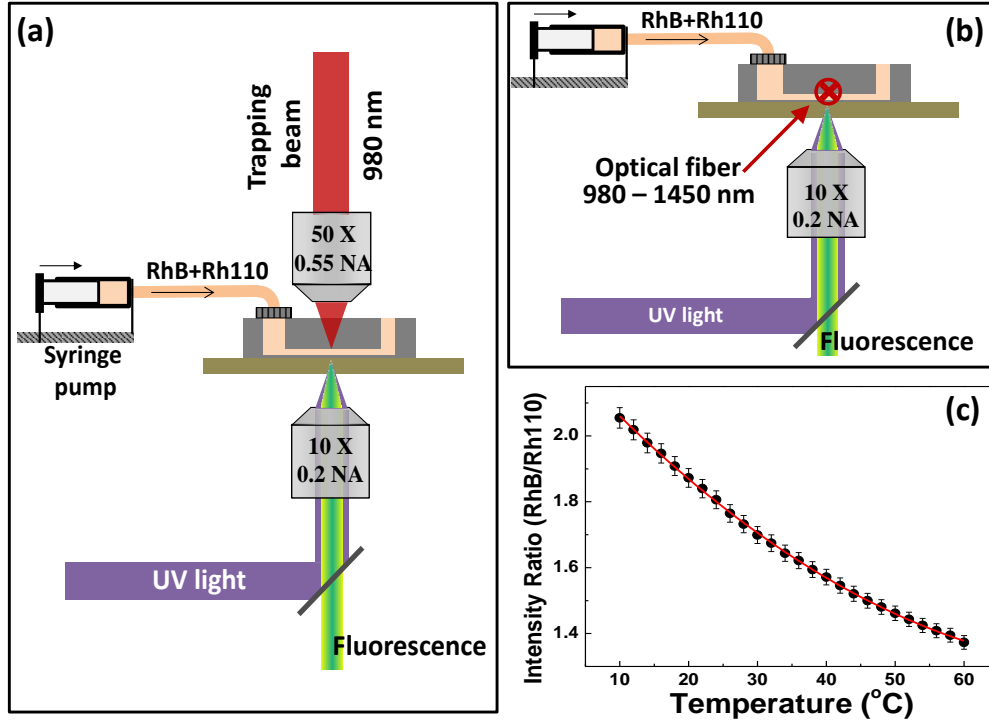


Fig. 2. Experimental setup and thermal calibration. (a) and (b) Schematic representation of the two experimental setups used for thermal imaging of the different optofluidic systems. (a) Optical trapping setup; (b) Setup for optofluidic devices with an on-chip fiber input for laser illumination. (c) Temperature dependence of the emitted intensity ratio of the two luminescent dyes (RhB and Rh110) used in this work.

As can be seen in Fig. 2(c), thermal quenching results in a decrease in the ratio between the emission intensities of both dyes, thus allowing us to determine the solution temperature with an accuracy of 1 °C in our experimental conditions. It should be noted that this estimated thermal accuracy has been found to be at least two times larger than the time-fluctuations in the measured temperature. As a consequence we concluded that the uncertainty in our thermal measurements is that estimated from the uncertainty associated to the calibration curve. Single point temperature measurements were carried out in a double-beam home-made confocal microscope. A continuous wave diode laser at 488 nm was used as an excitation source for the fluorescent dye solution. The laser radiation was focused into the microchannel by a 50X objective with a 0.55 numerical aperture, which led to a spot size of about 1 μm in diameter. This same objective was used to collect the luminescence from the dyes, which, after passing through appropriate filters, was spectrally analysed by a CCD camera attached to an iHR320 Horiba Jobin Yvon spectrometer.

To obtain two-dimensional thermal images of optofluidic devices, a commercial epi-fluorescence microscope was used. In this case, a high-voltage UV lamp acted as an excitation source for the fluorescent dyes, whose luminescence was separately recorded by using two different sets of fluorescence filters. These two fluorescence images were used to determine the spatial variation of the intensity ratio. In order to study the time evolution of the temperature distribution, two separate videos were recorded in order to obtain the signal from each dye; and the combined to obtain the final thermal images. Although this experimental setup provided us with the possibility of obtaining thermal images with reduced acquisition times, the thermal accuracy was estimated to be 2 °C, i.e. lower than that obtained when using the fluorescence confocal microscope described above. Therefore, the epi-fluorescence

microscope was used for obtaining two-dimensional thermal images, while the magnitude of the thermal loading was more accurately measured with the confocal microscope.

In all cases, the device holder was kept to a 20 °C temperature using a Peltier-cooled Linkam PE-120 temperature control stage.

For the purpose of optical excitation, two different laser sources were used, both being single-mode fiber coupled diodes operating at 980 and 1480 nm with maximum output powers of 500 and 200 mW, respectively. As is depicted in Fig. 2(a), for the purpose of optical trapping, an additional microscope objective (50X IR, 0.55 numerical aperture) was used for the optical trapping experiments (Fig. 1(a)). The 980 nm trapping beam was thus focused inside the microchannel, making sure that there was a match between the focal planes of the two microscope objectives represented in Fig. 2(a). The experimental setup used in the case of the three optofluidic chips (Figs. 1(b)-(d)) is schematically depicted in Fig. 2(b). The output of the diode laser (both the 980 nm and the 1480 nm) was coupled either to a multimode fiber (Thorlabs M42L01) inserted into the PDMS chips depicted in Figs. 1(b) and (c); or directly to the attached waveguide in the case of the device depicted in Fig. 1(d).

2.3 Mathematical modeling

COMSOL Multiphysics 4.3 was used to mathematically quantify the temperature increase within the optical trapping system at different flow rates. A 3D steady-state model was used to simulate the laser-induced temperature profile within the optical trap. Conjugated Heat Transfer (nitf) module was used here, considering the Gaussian beam optics as the heating source. The Navier–Stokes equation, the continuity equation and the heat transfer equation were coupled in COMSOL to solve the problem. Material properties were assumed to be constant over the temperature range. We set specific values as inlet velocities and also assumed no slip at the walls and incompressible fluid. Mathematical modelling was not performed on the side-pumped devices as, although possible, many experimental parameters (such as accurate fiber height in respect to micro-channel, optical losses at the fiber-device interface, and so on) are not accurately known so that results from modelling could not be fully reliable.

2.4 Lymphocyte preparation

For single-cell optical trapping experiments we used Jurkat cells (clone E6.1), a commercially available human T lymphocyte cell line from the American Type Culture Collection (ATCC), kindly provided by Drs V. Calvo and M. Izquierdo. Freshly cultured suspensions of these cells were maintained in RPMI 1640 medium supplemented with 10% fetal calf serum (FCS), 1% (v/v) penicillin/streptomycin (10 000 IU/mL/10 000 g/mL), and 2 mM L-glutamine (complete medium) in an incubator with humidified 95% air, 5% CO₂ atmosphere at 37 °C. All reagents were purchased from Fisher Scientific (Massachusetts, USA). For experiments, an aliquot of 100 μl of fresh, exponentially growing lymphocytes (cell density of 1 × 10⁶ cells/mL) were taken and subsequently diluted 1/5 with complete medium. Immediately afterwards 50 μL of this diluted suspension was placed on a microscopy chamber (Ibidi, Germany).

3. Results and discussion

3.1 Flow effects in the thermal loading of an optical trap

After properly calibrating our fluorescent thermal probe, determining the laser-induced thermal increment at the optical trap and its surroundings is a straightforward procedure. According to the simple model proposed by Mao et al., the thermal loading in an optical trap in the absence of fluid flow depends on the trapping beam parameters (laser power, P_i , and spot radius, R_i), on the thermal properties of the liquid medium (such as thermal diffusivity,

K) as well as on the absorption of the medium at the trapping wavelength $\alpha_{\text{abs}}(\lambda_{\text{trap}})$ and the chamber thickness, D , as given by expression (1) [29].

$$\Delta T_{\text{trap}} = \frac{\alpha_{\text{abs}}(\lambda_{\text{trap}}) \cdot P_l}{2\pi K} \cdot \ln\left(\frac{D}{R_l}\right) \quad (1)$$

In these experiments, the 980 nm diode laser was used. The water absorption coefficient at this wavelength is close to 0.5 cm^{-1} , so that a significant temperature increase is expected to occur. The experiments described in this section were all carried out under real trapping conditions, as supported by the image sequence included in Fig. 3(a), which corresponds to the optical trapping of a living cell (human lymphocyte) under these experimental conditions. In this case, the laser power was set to 300 mW, which corresponds to a power density of $340 \text{ mW}/\mu\text{m}^2$. Optical images included in Fig. 3(a) were only provided with the aim of demonstrating the optical trapping ability of our experimental setup. Nevertheless, during the recording of thermal images in presence of flow, the channel was only filled with the temperature-sensitive dye solution so that no particles were present either at the laser spot or in its surroundings.

The experimentally obtained thermal images of a 980 nm, 300 mW optical trap are presented in Fig. 3(b) as obtained at three different applied flows. Two main conclusions can be immediately extracted from these thermal images. First, the magnitude of the temperature increment is strongly dependent on the flow rate: the higher the flow rate, the lower the laser-induced heating. This is further evidenced in Fig. 3(c), where the maximum temperature increment is plotted as a function of the flow rate. The maximum heating corresponds to the static case, where the fluid at the focus of the optical trap experiences a temperature increase of about $21 \text{ }^\circ\text{C}$. This result is similar to that obtained in a previous work, where the heating rate in an optical trap under equivalent experimental conditions was found to be close to $99 \text{ }^\circ\text{C}/\text{W}$ [13]. The fact that the presence of a fluid flow reduces the thermal loading can be understood by taking into account that the effective heating time (time during which a fluid particle is in the laser focus) is reduced when the solution is flowing, consequently diminishing the magnitude of the temperature increment. It can be observed in Fig. 3(c) that the flow-induced reduction in the thermal loading follows a pseudo linear relation up to high flow rates close to $200 \text{ }\mu\text{L}\cdot\text{min}^{-1}$. For even higher flows, the temperature increment remains constant at about $6 \text{ }^\circ\text{C}$. This was unexpected, since it was assumed that high enough flow rates would cause the effective heating time to approach zero, consequently causing the induced temperature increment to be negligible. We attribute this discrepancy to the fact that, due to fluid viscosity, flow rate at the microchannel walls is zero and at those locations effective heating for any flow rate is produced, thus preventing complete heat dissipation.

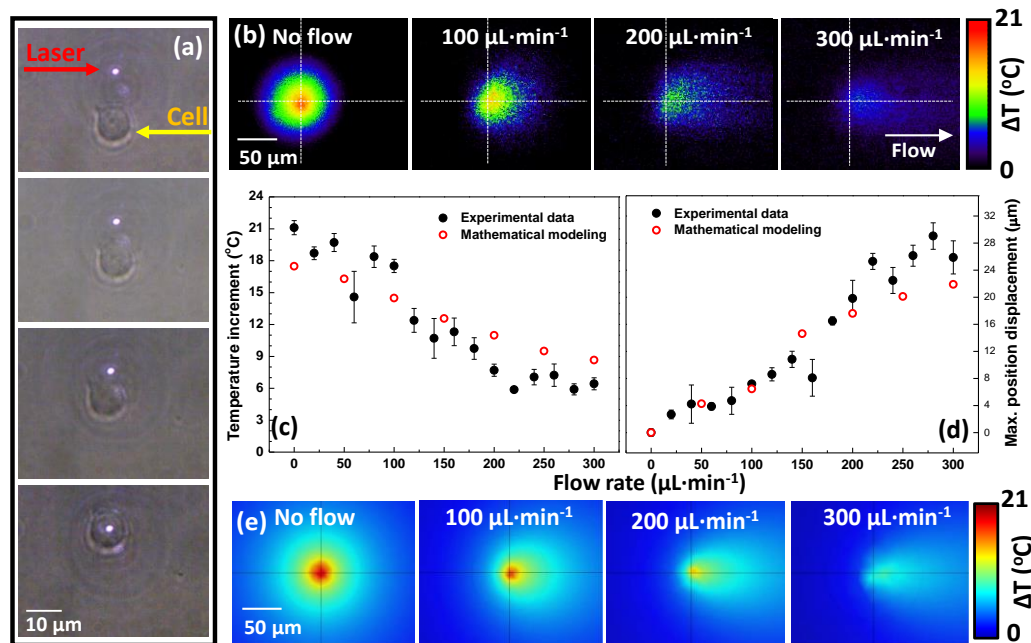


Fig. 3. (a) Image sequence recorded during the optical trapping of a human lymphocyte under a 980 nm trapping beam, with a set trapping power of 300 mW (b) Thermal loading in an optical trap at different flow rates. The trapping parameters were equal to those in Fig. 3(a). (c) and (d) Temperature increment and displacement of the maximum position at different flow rates for a 980 nm trapping power of 300 mW. Experimental results are indicated by dots, while empty circles represent the values predicted by numerical simulations. (e) Thermal images of an optical trap at different flow rates obtained from COMSOL modelling. The simulation conditions were set to match those of Fig. 3(b).

Applying a fluid flow does not only reduce the magnitude of the laser-induced thermal loading of an optical trap, but it also modifies the temperature distribution around the laser focus. As a matter of fact, an increase in the flow rate produces an elongation of the heat-affected area in the direction of the flow as can be observed in Fig. 3(b). This implies not only a change in the shape of the temperature distribution, but also a displacement in the position of the temperature maximum. As can be seen in Fig. 3(d), the location of temperature maximum overlaps the laser focus only in the static case, as even at low flow rates a shift in the maximum position is observed. As the flow rate increases, the distance between the warmest point and the trapping beam focus experiences a linear increase. A displacement as large as 30 μm is observed for the highest applied flow rates, corresponding to average linear speeds of about 0.5 cm/s. The fact that heat can be produced at a different location than that of the heating source (focused laser in our case) was an unreported phenomenon in locally heated microfluidics where a laser is acting as the heat source that could have relevant implications in the understanding of thermal dynamics of locally heated microfluidics.

Our experimental results are strongly supported by those yielded by COMSOL modeling. The thermal images predicted by the numerical simulation are shown in Fig. 3(e). It can be clearly seen that both the decrease in the thermal loading and the extension of the heat-affected zone, together with the maximum position displacement are predicted by the theoretical modelling of the optical trapping system. Furthermore, simulations do not only reproduce qualitatively the experimental data but they have also provided an excellent quantitative agreement. The numerical values predicted by the simulation for the temperature increment and the maximum displacement at four different flow rates (0, 100, 200 and 300

$\mu\text{L}\cdot\text{min}^{-1}$) have been included in Figs. 3(c) and (d), together with the experimental data. An excellent agreement is found in both cases. It should be noted that greater discrepancies between modelling and experimental data have been observed at high flow rates. We attribute this to the presence of fluid turbulences and instabilities at such large flow rates due to microchannel inhomogeneities. In addition we also think that such discrepancies are also due to the fact that for such high flow rates the magnitude of temperature increments is reduced and the modelling results become more critical on boundary conditions that are not fully controlled during experiments. Confirming the validity of our thermal imaging procedure, this encouraged us to apply the same method to perform time-resolved thermal imaging in an optical trap. Thermal images included in Fig. 3 were obtained 20 seconds after switching on the laser, thus making sure that a steady state, i.e. a stable temperature distribution, had been reached. Nevertheless, that temperature distribution around the laser focus is not expected to be achieved in an instantaneous manner. Indeed, the characteristic time of a thermal process, t_T , can be roughly estimated by applying dimensional analysis to the heat transport equation, and can be demonstrated to be given by:

$$t_T = L^2/K \quad (2)$$

where L is characteristic size of the system and K is the thermal diffusivity of the medium ($0.143 \times 10^{-6} \text{ m}^2/\text{s}$ for water) [30]. Note that t_T is defined as the time required for the temperature to rise up to 63% of the steady state increment (i.e. defined on the basis of the $1/e$ criteria). For rectangular channels, it can be assumed that the characteristic length is equal to the channel height, h , so that expression (2) predicts a faster thermal stabilization for thinner microchannels. Figure 4 shows the time evolution of the normalized on-focus temperature as obtained when the 980 nm laser beam was focused inside 100 and 200 μm high channels in absence of fluid flow.

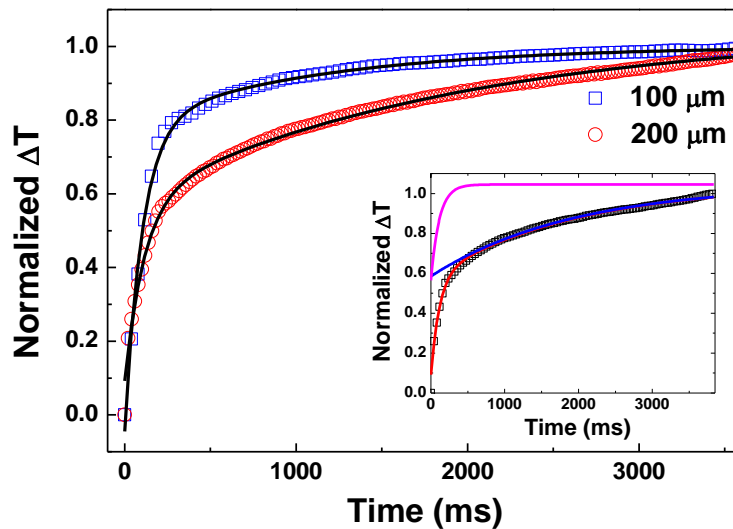


Fig. 4. Thermal loading in an optical trap generated by a 980 nm laser beam as obtained for two different channel heights (100 and 200 μm). Dots are experimental data and solid lines are the best fits to a double exponential function. Inset includes the heating curve obtained in the 200 μm showing the two exponential curves resulting from the fitting procedure.

As can be observed, thermal stabilization on the 100 μm high channel happened much faster than on the 200 μm high one. Indeed the stabilization times (estimated following the $1/e$ criterion) were found to be 180 and 790 ms for the 100 and 200 μm high channels, respectively. This experimental observation is in qualitative agreement with expression (2).

Nevertheless, the thermal transients were found not to follow a single exponential as was expected. Instead, they can be well described by a double exponential function. This is evidenced in the inset of Fig. 4, where the thermal transient obtained for a 200 μm height channel is represented together with the two exponential growth curves which best fit our experimental data. The characteristic times of these exponentials are close to 100 ms and 1 s. These times can be compared to those given by expression (2), which for a 200 μm high channel predicts a characteristic time of 270 ms. Note that expression (2) has been derived from the heat transport equation, considering that convection currents do not occur in the fluid and that contour conditions/temperatures are fixed. We state at this point that the experimentally observed fast component of the thermal transient corresponds to the time required for the thermalization of the fluid itself, whereas the slow component arises from both the appearance of convection currents and the modification of contour conditions / temperatures (i.e. corresponds to the time required for contour thermalization). This tentative assignment is in good agreement with the fact that the relative weight of the slow component clearly decreases when the channel height is reduced down to 100 μm (see Fig. 4).

Data included in Fig. 4 correspond to static conditions, i.e. in the absence of fluid flow. Nevertheless, it has been observed that the presence of a fluid flow leads to a drastic modification in the thermal transients. This is evidenced in Fig. 5, which includes the time evolution of the maximum trap temperature as obtained in a 100 μm height channel at three different flow rates. Note that, as the flow rate increases, the relative contribution to the thermal transient of the slow component decreases. This decrease has been found to be monotonic with the applied flow rate, as can be observed in the inset of Fig. 5, where the ratio between the amplitudes of the slow and fast components of the thermal transients (A_{slow} and A_{fast} , respectively) is represented. Indeed, for flow rates close to 150 $\mu\text{L}\cdot\text{min}^{-1}$ (corresponding to an average linear speed of 0.5 cm/s), the thermal transient is well described by a single exponential with a characteristic time close to 80 ms. This is, in fact, very similar to the characteristic time given by Eq. (2) for a 100 μm high channel; $t_T \approx 70$ ms. We state that, for such high flow rates, the appearance of convection currents is prevented. In addition, the presence of fluid flow reduces the magnitude of intrachannel heating (see Fig. 3(c)) and, consequently, minimizes possible changes in contour conditions/temperature. Experimental data included in Fig. 5 demonstrate the critical role played by the flow rate in the time evolution of thermal processes in optofluidic devices. Such a critical role has not been discussed before and would be of importance for the proper understanding of transient phenomena. In addition, the transient thermal curves here reported could open the possibility of novel approaches (such as modulation of laser/heating sources) for full control and minimization of thermal effects in optofluidic devices.

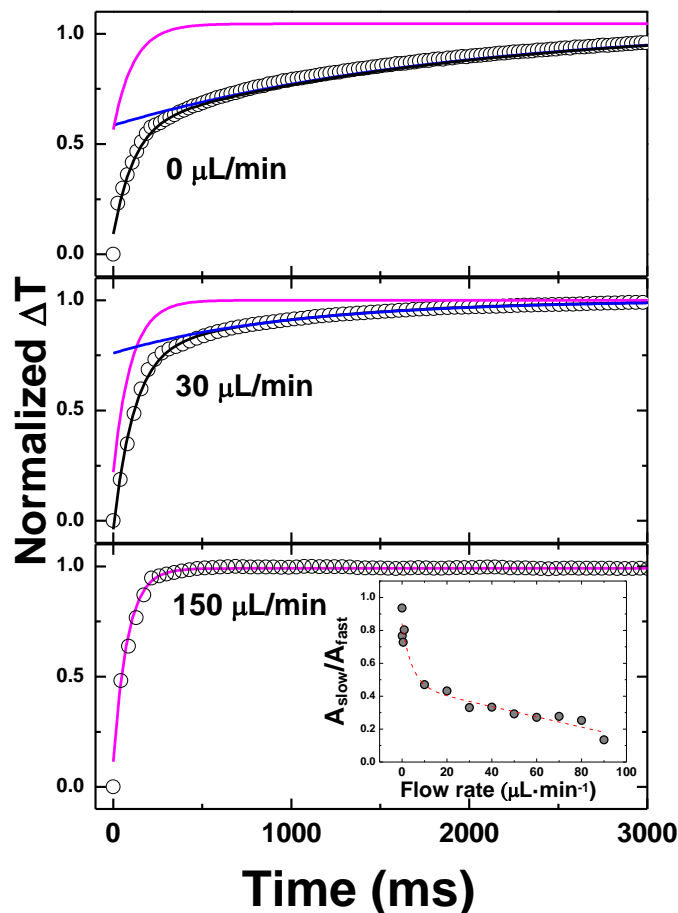


Fig. 5. Time evolution of the temperature of an optical trap generated by a 980 nm laser beam focused in a 100 μm high channel as obtained for three different flow rates. Dots are experimental data and solid lines are the best fits to a double or single exponential function. The fast and slow components are also plotted in each case. Inset shows the relative contribution of the slow component for different flow rates. Dots are experimental data and the dashed line is added for clarity.

3.2 Thermal loading in optofluidic chips for particle manipulation

Flow-related effects analogous to those reported in the previous section for single beam optical traps are also expected to occur in the optofluidic devices depicted in Figs. 1(b)-(d). In order to corroborate this, we have obtained thermal images for all the devices under real operating conditions using 980 nm and 1480 nm fiber coupled laser diodes. Laser radiation at 1480 nm was used to obtain intense and easy to record thermal effects even at high flow rates as at this particular wavelength water absorption coefficient is as large as 28 cm^{-1} , i.e.; more than 50 times the water absorption coefficient at 980 nm (0.5 cm^{-1}). Evidence of the higher thermal loading when replacing the 980 nm diode with the 1480 nm one is provided in Fig. 6(a), which shows thermal images of the temperature increment in a straight microchannel side-pumped by an optical fiber as is schematically depicted in Fig. 1(b). All images in Fig. (6) were recorded 2 seconds after the laser had been turned on, so that a stable temperature distribution had been reached.

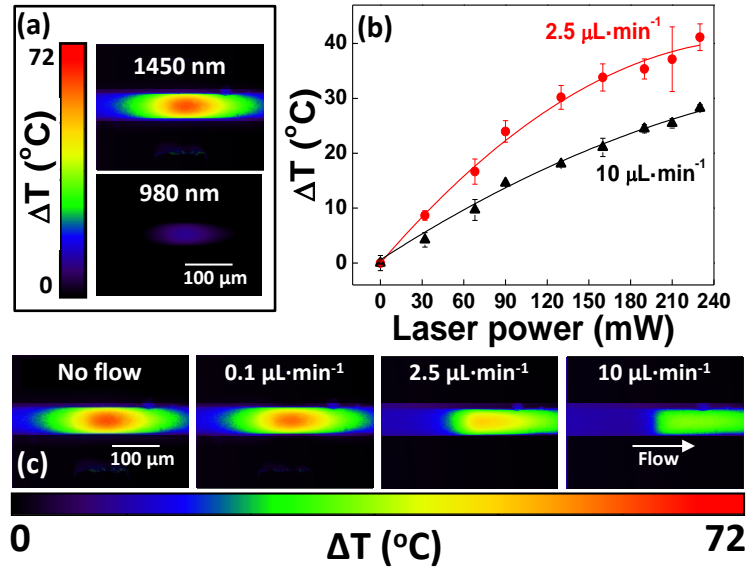


Fig. 6. Effect of flow rate and irradiation wavelength on the thermal loading in the microchannel depicted in Fig. 1(b). (a) Thermal images obtained under 130 mW trapping beam power at two different wavelengths: 1480 nm and 980 nm. (b) Maximum temperature increment in the microchannel as a function of the laser power for 1480 nm trapping beam power at two different flow rates. (c) Thermal images obtained under 1480 nm irradiation (130 mW laser power) at four different flow rates.

As can be observed, pumping at 980 nm resulted in a temperature increment of few degrees Celsius, thus complicating flow-dependent temperature measurements. When pumping at 1480 nm, a very high contrast temperature pattern is obtained. Note that, under static conditions, temperature increments above 70°C occur at 1480 nm laser powers of 130 mW. It is important to note that, in all cases, we are referring to launched laser powers, as the actual power reaching the microchannel is difficult to estimate due to the fact that the actual coupling losses are not known. However, due to the low absorption coefficient of PDMS at these wavelengths [31], most of the launched laser power is expected to reach the microchannel. The temperature increments observed in absence of any flow can be compared to those reported for side-pumped microfluidic devices filled with an aqueous solution containing carbon nanotubes. In those cases a 150 mW, 980 nm laser beam induced a local increment close to 25°C [24]. For such large thermal gradients, convection currents are expected to occur. We state that the presence of such convection currents results in the temperature increment no longer being linearly proportional to the laser power (see Fig. 6(b)). The initially expected linear relation was only observed when flow rates were higher than $10 \mu\text{L}\cdot\text{min}^{-1}$. The establishment of such high flow rates does not only lead to a thermal loading proportional to the laser power but also to the creation of highly asymmetric thermal patterns as can be observed in Fig. 6(c). Note that, for a flow rate of $10 \mu\text{L}\cdot\text{min}^{-1}$, the intrachannel temperature follows a step-like evolution. The 1480 nm laser beam creates two spatial regions with very well defined temperatures. These particular thermal patterns could be useful for controlled photothermal studies or for the creation of unidirectional thermal forces at the position of the laser beam. From Fig. 6(b), it is also clear that, for a given laser power, the magnitude of thermal loading decreases with the applied flow rate, as it was also observed in the experiments regarding the thermal loading of a single laser beam optical trap. Again, flow rate is evidenced as a heat dissipation source.

Experiments similar to those included in Fig. 6 were also performed on the side-pumped microchannel fabricated by ultrafast inscription in fused silica (device depicted in Fig. 1(d)). We found, qualitatively, the same behaviour as was observed in the PDMS-based device.

The time evolution of the thermal patterns created by the 1480 nm laser beam in the optofluidic device depicted in Fig. 1(b) has also been investigated and results are summarized in Figure 7. Figure 7 (a) shows the thermal images at different times after switching the laser on, as obtained in the presence and absence of fluid flow. The time evolution of the maximum temperature increment is shown in the absence of fluid flow (Fig. 7(b)) and with a flow rate of $1 \mu\text{L}\cdot\text{min}^{-1}$ (Fig. 7(c)).

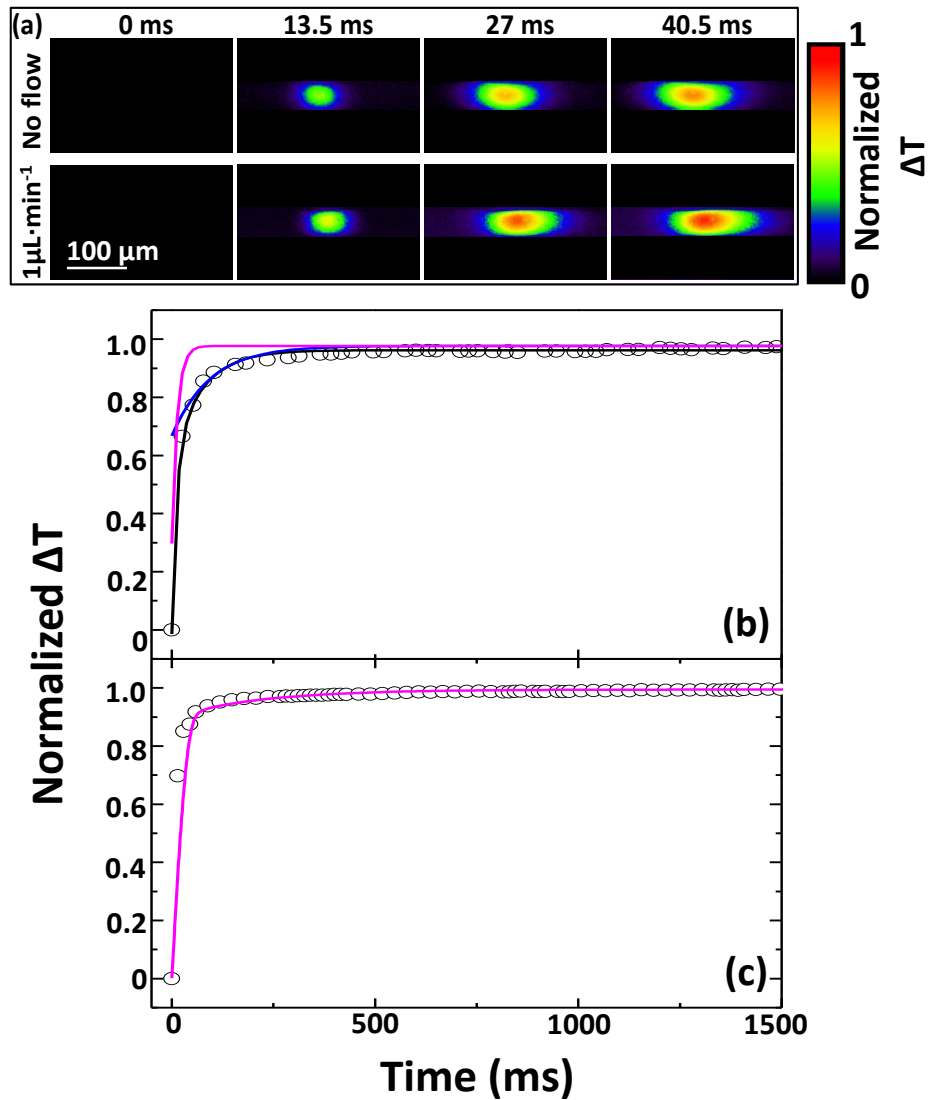


Fig. 7. (a) Time evolution of the temperature distribution created in the channel depicted in Fig. 1(b). Thermal images are represented for different times after the 130 mW laser power at 1480 nm was turned on. Scale bar is $100 \mu\text{m}$. (b) Time evolution of the normalized temperature increment in the microchannel in the static case and (c) under an applied flow of $1 \mu\text{L}\cdot\text{min}^{-1}$.

On a first inspection, a much faster thermal stabilization than that experimentally observed for the optical trap (see Figs. 4 and 5) is observed. This was indeed expected, as the reduced dimensions of the device lead, according to expression (1), to shorter stabilization times. Again, following the $1/e$ criterion, we estimated a thermal stabilization time in the static case equal to 31 ms, significantly smaller than that obtained for the optical trap (180 ms). As in the case of the thermal loading in an optical trap, the thermal transient in static conditions is well described by a double exponential growth function (see solid lines in Fig. 7(b)). Also, the fast component is once again related to the thermal stabilization of the fluid, while the slow component is associated with the time required for the stabilization of flow currents and of contour conditions. In this case the amplitude of the slow component is ten times lower than that of the fast component, in contrast to the experimental results obtained for the optical trap (Fig. 5) in which, under static conditions, both components contributed with the same amplitude to the net transient. We state that the reduced dimensions of the channel minimize the presence of convection currents, therefore decreasing their contribution to the thermal transient. Figure 7(c) shows that, when a flow rate is applied, the time required for the temperature distribution to stabilize becomes shorter, as was already observed in the case of the optical trap. Indeed, as can be observed in Fig. 7(c), even with an applied flow rate of $1 \mu\text{L}\cdot\text{min}^{-1}$, the thermal transient can be well described with a single exponential. According to our previous discussion, this implies that the presence of such flows minimizes the contribution of convection currents to the thermal stabilization. Indeed, from the single exponential fit, we have obtained a characteristic thermal stabilization time of 10 ms. If we assume $50 \mu\text{m}$ as the characteristic length of these devices, the value predicted by expression (1) is 17 ms, which is quite close to the experimentally determined value.

Finally, thermal loading in the optofluidic device fabricated for particle sorting schematically drawn in Fig. 1(c) has also been investigated. In this device, the particles to be manipulated are injected through one of the input channels. When particles reach the junction area they are subjected to 980 nm laser radiation and, due to scattering forces, controlled sorting is produced. Figure 8(a) shows an optical transmission picture of the sorting device. The trajectories followed by polystyrene beads $7 \mu\text{m}$ in diameter injected through one of the input channels in the presence of a 980 nm laser beam focused into the junction area are drawn. As can be observed, particle sorting with an efficiency close to 75% has been observed.

Data included in Fig. 8(top) were obtained under illumination at 980 nm (laser power of 450 mW) at an applied flow rate of $0.02 \mu\text{L}\cdot\text{min}^{-1}$, corresponding to an average linear speed of $100 \mu\text{m}/\text{s}$. It was found that the sorting efficiency decreases dramatically if the laser power was decreased or the input flow rate was increased. The thermal images of the sorting device as obtained for different flow rates and at different times after switching on the laser are included in Fig. 8. In all the cases, thermal images were obtained at 450 mW laser power. From the thermal images, it is clear that the maximum temperature increment induced in the sorting device was 5°C under operating conditions. Once again, the increase of the fluid flow rate results in a dramatic reduction of this heating. Note that even at the low flow rates required for effective microparticle sorting (flow rates well below $0.1 \mu\text{L}\cdot\text{min}^{-1}$) the temperature increment produced at the junction area is no higher than 5°C . This is a critical number for bioapplications since if the device is operating at 37°C then 5°C laser induced heating would lead the fluid to the limit of the biophysical temperature range (42°C).

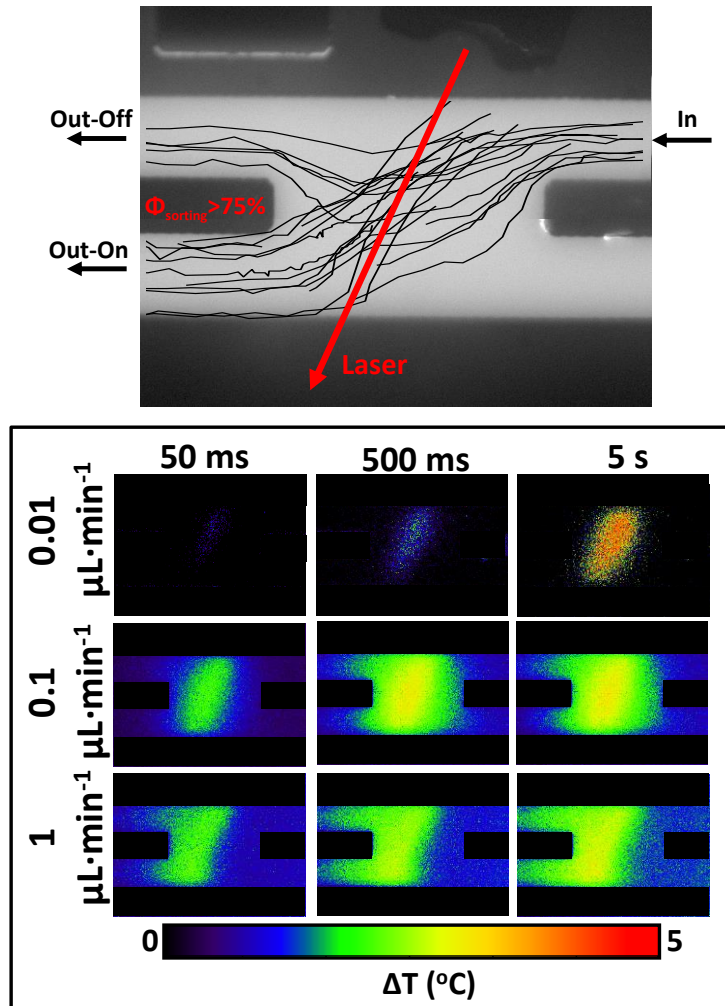


Fig. 8. Top. Trajectories of microparticles circulating through the sorting channel depicted in Fig. 1(c) at a laser power of 450 mW. Bottom. Thermal loading in the sorting device at three different times (50 s, 500 ms and 5 s) after the 980 nm laser beam has been turned on at three different flow rates (static, 0.1 and 1 $\mu\text{L}\cdot\text{min}^{-1}$).

As was observed for the previously described optofluidic systems, the time required for the temperature to stabilize is shorter for higher flow rates. Nevertheless, we have found the thermal stabilization time in the sorting device under real operating conditions to be shorter than 500 ms. Finally, it should be noted that higher flow rates also result in a great asymmetry in the temperature distribution, so that the temperature at the output channels is higher than that at the input channels.

6. Conclusions

Thermal loading of optofluidic devices is a known and sometimes unavoidable effect due to the presence of water absorption bands at certain laser wavelengths. Several works have reported on laser-induced intrachannel temperature changes, but little was known about the effect that the presence of fluid flow has on the magnitude, spatial extension and stabilization time of the laser induced thermal patterns. In this work, we have provided experimental evidence on how the establishment of a fluid flow dramatically changes the spatial

distribution and dynamics of intrachannel heating. We have systematically investigated the case of single beam optical traps. It has been found that the fluid flow behaves as an additional dissipation source reducing the magnitude of thermal loading. In addition, it causes a drastic distortion of the temperature pattern, leading, for example, to a spatial displacement between the laser focus and the hottest point in an optical trap. Flow rate has also been found to be crucial in determining the time required for thermal stabilization. When a flow rate is applied, the time required to reach a stable temperature distribution becomes shorter due to the elimination of convection currents by laminar flow rates.

By measuring thermal images of different optofluidic devices we have found that the main features observed in single beam optical traps are reproduced in more complex optofluidic devices based on PDMS and fused silica.

Results included in this work put in context the importance of flow rate in the thermal dynamics of optofluidic devices and would be of great importance in their understanding, design and use.

Acknowledgments

This work has been supported by the Spanish Ministerio de Educacion y Ciencia (MAT2010-16161 and MAT2013-47395) and by Universidad Autónoma de Madrid and Banco Santander. B. del Rosal acknowledges Universidad Autónoma de Madrid for an FPI-UAM grant. Y. Yan acknowledges the funding support from SINAPSE. This work has received funding from The Royal Society (IE130466). M. Mackenzie acknowledges funding from EPSRC (grant no EP/J500227/1).